NeuroImage 52 (2010) 1123–1134

Contents lists available at ScienceDirect

NeuroImage

journal homepage: www.elsevier.com/locate/ynimg

A parallel framework for simultaneous EEG/fMRI analysis: Methodology and simulation

Xu Lei, Chuan Qiu, Peng Xu, Dezhong Yao *

The Key Laboratory for NeuroInformation of Ministry of Education, School of Life Science and Technology, University of Electronic Science and Technology of China, Chengdu, 610054, China

ARTICLE INFO

Article history:
Received 31 July 2009
Revised 23 December 2009
Accepted 11 January 2010
Available online 18 January 2010

Keywords:
EEG/fMRI
Multimodal imaging
Fusion
Empirical Bayesian
Source imaging
HRF estimation

ABSTRACT

Concurrent EEG/fMRI recordings represent multiple, simultaneously active, regionally overlapping neuronal mass responses. To address the problems caused by the overlapping nature of these responses, we propose a parallel framework for Spatial–Temporal EEG/fMRI Fusion (STEFF). This technique adopts Independent Component Analysis (ICA) to recover the time-course and spatial mapping components from EEG and fMRI separately. These components are then linked concurrently in the spatial and temporal domain using an Empirical Bayesian (EB) model. This approach enables information one modality to be utilized as priors for the other and hence improves the spatial (for EEG) or temporal (for fMRI) resolution of the other modality. Consequently, STEFF achieves flexible and sparse matching among EEG and fMRI components with common neuronal substrates. Simulations under realistic noise conditions indicated that STEFF is a feasible and physiologically reasonable hybrid approach for spatiotemporal mapping of cognitive processing in the human brain.

Introduction

Functional magnetic resonance imaging (fMRI) noninvasively measures local hemodynamic changes associated with neuronal activity. An unresolved issue in fMRI research is the limited temporal resolution of the blood oxygenation level dependent (BOLD) response. In contrast to the poor temporal resolution of fMRI, electroencephalogram (EEG) measurements can instantaneously record the electrophysiological signal produced by synaptic activity. However, due to the 'inverse problem' inherent in EEG recording (Helmholtz, 1853), the spatial location of the neural generators of observed activity cannot be conclusively determined (Baillet et al., 2001; Lei et al., 2009a). The fusion of these two complementary noninvasive methods would allow for the combined high-resolution spatial and temporal mapping of mental processes. Such a technique could provide a more comprehensive understanding of the neural correlates of perception and cognition (Ives et al., 1993; Dale and Halgren, 2001; Debener et al., 2006; Ritter and Villringer, 2006).

Physiologically, simultaneous EEG/fMRI recordings constitute volume-conducted and hemodynamically convolved signals from neural events that are spatially and temporally 'mixed' across the brain. That is, the observed data in both modalities represents responses from multiple, simultaneously active, regionally overlapping neuronal populations (Baudena et al., 1995). Scalp EEG recordings sample a spatially degraded map of neural activity, and a temporal mixture of independent time-courses from large-scale synchronous field potentials (Makeig et al., 2004). fMRI involves several equivalent constraints, providing temporally degraded and spatially mixed signals by measuring the neurovascular transformation of neural activity (Calhoun and Adali, 2006). Independent component analysis (ICA) is potentially an ideal approach to address this mixing problem and has been applied successfully to a variety of problems in EEG (Makeig et al., 2004) and fMRI recording (McKeown et al., 1998; Calhoun et al., 2001; Chen and Yao, 2004; Beckmann and Smith, 2004).

EEG/fMRI fusion is typically based on the assumption that the hemodynamic response is linearly related to local changes in neuronal activity and, in particular, to local field potentials (Logothetis et al., 2001). Large-scale synchronous field potentials underlie the electrophysiological signal recorded by scalp EEG (Nunez, 1995). Consequently, a method for integrating the two approaches may be developed by determining the relation between the BOLD signals measured by fMRI and the electrophysiological measures provided by EEG, either in the spatial or temporal domain.

There are currently three broad potential approaches to EEG/fMRI integration: (i) 'symmetric fusion', where a common generation model is constructed to explain both the EEG and fMRI data (Daunizeau et al., 2007; Deco et al., 2008; Valdes-Sosa et al., 2009); (ii) 'spatial constraint', where spatial information from fMRI recordings is used for source reconstruction of the EEG data (Liu et al., 1998; Dale et al., 2000; Trujillo-Barreto et al., 2001; Lei and Yao, 2009) and (iii) 'temporal prediction', where the fMRI signal is modeled with

* Corresponding author. Fax: +86 28 83208238.
E-mail address: dyao@uestc.edu.cn (D. Yao).

1053-8119/$ – see front matter © 2010 Elsevier Inc. All rights reserved.
doi:10.1016/j.neuroimage.2010.01.024

data from certain EEG measures, convolved with a hemodynamic response function (HRF; Martinez-Montes et al., 2004; Debener et al., 2006; Eichele et al., 2008a; Moosmann et al., 2008).

In temporal prediction, various features of the EEG signal can be used as measures of interest, such as alpha power (Goldman et al., 2002) and P300 amplitude (Eichele et al., 2005; Warbrick et al., 2009) among others. EEG data can be convolved with a canonical HRF, the result of which can be used as a hemodynamic predictor in a general linear model (GLM). This approach has been adopted in the study of spontaneous brain rhythms (Goldman et al., 2002), epileptic discharges (Laufs et al., 2008), and the inducing amplitude variation in a cognitive task (Debener et al., 2006). For spatial constraint, in order to extend the fMRI-constrained EEG inversion (Liu et al., 1998; Dale et al., 2000), we recently proposed an EEG source reconstruction method based on fMRI connectivity patterns. This technique, termed 'network-based EEG source imaging' (NESOI), uses multiple spatially independent maps (or networks) derived from fMRI as covariance priors for EEG source reconstruction (Lei and Yao, 2009).

The spatial constraint and temporal prediction approaches described above do not consider EEG and fMRI data sets equivalently or analyze them jointly. The goal of these methods is typically either spatial localization or temporal dynamic reconstruction, in which one modality is given privileged status as a prior for the other modality (Valdes-Sosa et al., 2009). Thus, they are examples of asymmetrical EEG/fMRI integrations. In contrast, symmetrical fusion does not assign an a priori inferential preference to any given modality (Trujillo-Barreto et al., 2001). The existing symmetrical fusion based on a cascade of generation models may provide a deeper understanding of the neural mechanisms underlying mental processes of interest (Daunizeau et al., 2007; Deco et al., 2008; Valdes-Sosa et al., 2009). However, current generative model-driven symmetrical methods employ highly detailed large-scale computational modeling and require the explicit definition of the common neuronal substrates that elicit both EEG and fMRI measurements. However, the lack of precise knowledge about neural mechanisms has led to a reduced scope for the application of these techniques.

In contrast to the generative model-driven fusion which exploits models of the chain of events leading to observed measurements, data-driven fusion is based on measuring mutual dependence between the two modalities (Valdes-Sosa et al., 2009). In this approach, original EEG/fMRI data are typically first decomposed into components, then matched to each other (Calhoun et al., 2009). Blind source separation has been used to address the mixing problems of EEG/fMRI using parallel ICA (Eichele et al., 2008a) and joint ICA (Moosmann et al., 2008). Eichele et al. (2008a) performed integration with simple pair-wise matching of across-trial modulation. In a study by Moosmann et al. (2008), the components linking both modalities were estimated using decomposition of the joint data space. The key strength of data-driven fusion is its ability to remove noise from the data, generate priors and provide group inferences that can serve as constraints for model-driven methods. Hence data-driven techniques are helpful in localizing the generators of EEG phenomena and informing models of interaction among levels of cortical hierarchies (Garrido et al., 2007). Furthermore, data-driven approaches may provide a solution to the problems faced by neurovascular transformation function estimation. This may clarify the relationship between the electrophysiology of neuronal systems and their slower hemodynamics in terms of their individual forward models (Deco et al., 2009).

Methodological and conceptual developments in the field of multimodal integration are ongoing, and the need for a more flexible model is one of the outstanding challenges for EEG/fMRI integration (Eichele et al., 2009). In the current study, we adopted a hybrid approach, where data-driven blind source separation (group ICA) was cascaded with an EEG forward model and a neurovascular transformation convolution model for neural source estimation and hemodynamic response function reconstruction. We term this approach Spatial-Temporal EEG/fMRI Fusion (STEFF). STEFF is not based on a common generative model, but employs constraints and predictions in an unmixed space. In STEFF, two asymmetric fusion methods, spatial constraint and temporal prediction, are implemented in parallel. Information from one modality is used to generate priors for the other modality and the matching between components is estimated using variational Bayesian inference. Here we present the details of the STEFF approach and the results from simulated data under realistic noise conditions.

Method

As the first step of the STEFF approach, we subject EEG and fMRI data to modality-specific preprocessing to allow for later group inferences (e.g., spatial normalization of individual fMRI volumes, ICA-based artifact removal of EEG; see Fig. 1 for schematic overview). Principal component analysis (PCA) is then adopted to compress the data on single subject level. Single subject data are concatenated in an aggregate set. Temporal ICA (tICA) and spatial ICA (sICA) are performed on EEG and fMRI data, respectively, and subject-specific

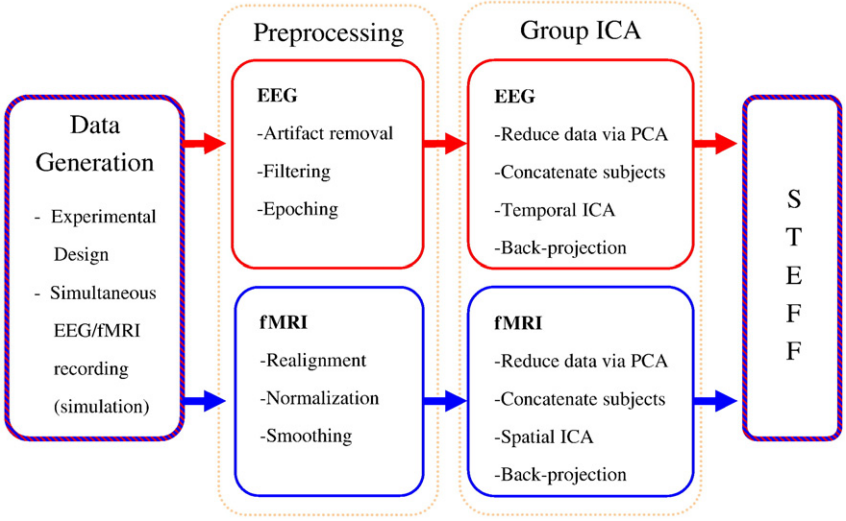

Fig. 1. Illustration of the unified framework for simultaneous EEG/fMRI analysis. EEG and fMRI data first undergo modality-specific preprocessing. Group ICA is then implemented in each modality. Finally, EEG and fMRI independent components are matched using STEFF.

maps and time-courses are reconstructed by back-projecting the independent components. Finally, components are averaged over subjects and matched across modalities by STEFF. The details of these procedures are listed below.

The above steps for real data can be implemented in MATLAB (www.mathworks.com) with the academic freeware toolboxes EEGLAB (http://sccn.ucsd.edu/eeglab), GIFT (http://icatb.sourceforge.org), and SPM8 (http://www.fil.ion.ucl.ac.uk/spm). In our computer simulation, the code for data generation and visualization, and the simulated data used here were collected in a customized STEFF toolbox which is available from the authors upon request.

Data preprocessing

Under real conditions, data transformations are necessary to remove data with low repetition to increase the signal-to-noise ratio. For fMRI data, the implemented steps typically include transforming individual anatomy to a standardized space, correcting head motion related image offsets, and temporal filtering. These pre-processing steps can be implemented using SPM8. For the EEG data, these steps correspond to correcting for gradient and cardiobalistogram artifacts (Allen et al., 2000; Niazy et al., 2005), band-pass filtering and re-referencing (Yao, 2001; Yao et al., 2005). A MATLAB-based toolbox for this purpose is available in EEGLAB. In the current study, we used simulation to evaluate the performance of STEFF, avoiding these preprocessing steps.

Group ICA

The group EEG/fMRI decomposition includes a group temporal independent components analysis (tICA) of EEG data and group spatially independent components analysis (sICA) of fMRI data. A comprehensive description of group ICA can be found in Calhoun et al. (2001), and its implementation for real data are publicly available in GIFT software (GIFT, 2008). The main points are summarized as follows: data from all subjects are combined into a single data matrix after dimension reduction. The resulting data matrix is decomposed into N components. In order to determine the number of components, dimension estimation is performed using the minimum description length criteria (Li et al., 2007). Single subject independent components and mixing matrices are then computed using back-reconstruction.

For a single subject, the independent component matrix contains the N components (sIC in fMRI and tIC in EEG) and the mixing matrix consists of fMRI time-courses (or EEG topographies) corresponding to the N components. The results of the above procedures formed the basis of parallel fusion of EEG and fMRI, as shown in Fig. 2.

For each modality, the resulting components are subjected to random effects analyses. Common independent components (ICs) among the subjects are inspected and identified for the following subsequent parallel fusion. For the ith fMRI sIC of the first subject, we calculate the correlation coefficients (CC) between the ith fMRI time-course and that of all the components from all other subjects. For each component, if more than half the subjects' maximum CCs are higher than 0.8, this component is retained and averaged across these subjects as a group component. The corresponding components in these subjects are then discarded in the calculation of the next group components. For the first subject, this calculation is executed from $i=1$ to N and the corresponding group components are discarded. The calculation is then executed for the remaining components for the remaining subjects. The averaged time-courses (group components) are filtered with a 128-second high-pass Butterworth digital filter and normalized to unit variance. These grand averaged time-courses are adopted as the BOLD signals from sIC active areas for HRF estimation. For each EEG tIC, similar steps are taken, and the final group averaged topographies serve as scalp EEG recordings for EEG source imaging. For the following STEFF procedure, as shown in Fig. 2, the components adopted are group averaged fMRI sICs, their time-courses, group averaged EEG tICs, and the corresponding topographies.

STEFF

After acquiring the group maps and time-courses for both EEG and fMRI, STEFF provides constraint and prediction integration in parallel, in an unmixed IC space (Fig. 2). For 'fMRI-constrained EEG imaging', to find the voxel-wise description of the topography of an EEG tIC, fMRI sIC patterns are typically employed as the covariance priors for EEG source distribution. For 'EEG-informed HRF estimation', the trial-by-trial dynamics (single trial quantification in Fig. 2) extracted from EEG tIC act as the prediction information and form the design matrix for fMRI HRF estimation. Both of these approaches are described below.

fMRI-constrained EEG imaging (left dashed area in Fig. 2)

For the group averaged topography of each EEG tIC, Y_e, we employ an Empirical Bayesian (EB) model (Phillips et al., 2005; Friston et al., 2006) for its underlying source distribution,

$$\begin{array}{ll} Y_e = X_e\Phi_e + E_{1e} & E_{1e}\tilde{}N(0, C_{1e}) \\ \Phi_e = 0 + E_{2e} & E_{2e}\tilde{}N(0, C_{2e}), \end{array} \quad (1)$$

where $Y_e \in R^{n\times 1}$ is one of the p tIC EEG topographies with n channels. $X_e \in R^{n\times d}$ is the known lead-field matrix calculated for the selected head model, and $\Phi_e \in R^{d\times 1}$ is the unknown distribution of d dipoles. $N(\mu C)$ denotes a multivariate Gaussian distribution with mean μ and covariance C. The terms E_{1e} and E_{2e} represent random fluctuations in channel and source spaces, respectively. These spatial covariances E_{1e} and E_{2e} are mixtures of covariance components at the corresponding levels. At the sensor space level, we assume $C_{1e}=\alpha^{-1}I_n$ to encode the covariance of sensor noise, where I_n is an $n\times n$ identity matrix. At the source space level, we express C_{2e} as the covariance components,

$$C_{2e} = \sum_{i=1}^{k} \gamma_i V_i, \quad (2)$$

where $\gamma \equiv [\gamma_1, \gamma_2, \ldots, \gamma_k]^T$ is a vector of k non-negative hyperparameters that control the relative contribution of each covariance basis matrix, V_i. The Green function, $G=2\exp(A)$, models anatomic coherent sources and is a function of an adjacency matrix, A, with $A_{ij} \in [0,1]$ encoding the neighboring relationships among nodes of the cortical mesh defining the solution space (Harrison et al., 2007). The jth column of the Green function matrix G is q_j, encoding neighboring patches weighted by their surface proximity (Friston et al., 2008).

STEFF employs two different kinds of covariance matrices, i.e.,

$$\{V_i\} = \left\{V_i^{\mathrm{f}}\right\} \cup \{V_i^{\mathrm{e}}\}, \quad (3)$$

where V_i^{f} encodes the prior coherence pattern information derived from fMRI (Lei and Yao, 2009) and V_i^{e} encodes multiple sparse priors (Friston et al., 2008) that are sparsely sampled from a subspace of EEG source space that does not contribute to fMRI measurements. The intensity values in each fMRI sIC are scaled to z scores. Voxels with absolute z scores of >3 are considered to show activation. Negative z scores indicate that the BOLD signals are modulated oppositely to the IC waveform (McKeown et al., 1998). A node in the EEG source space is assigned according to the z score of its nearest-neighbor fMRI voxel after spatial registration. All the activated nodes (absolute z scores >3) in each IC show similar temporal dynamics of the BOLD signal, thus we assume they have similar properties for EEG signal generation. The simplest way to construct a covariance component from an IC is to assign the diagonal terms by 1.0 if the corresponding node is activated, and assign the other terms by 0.0. STEFF takes into account

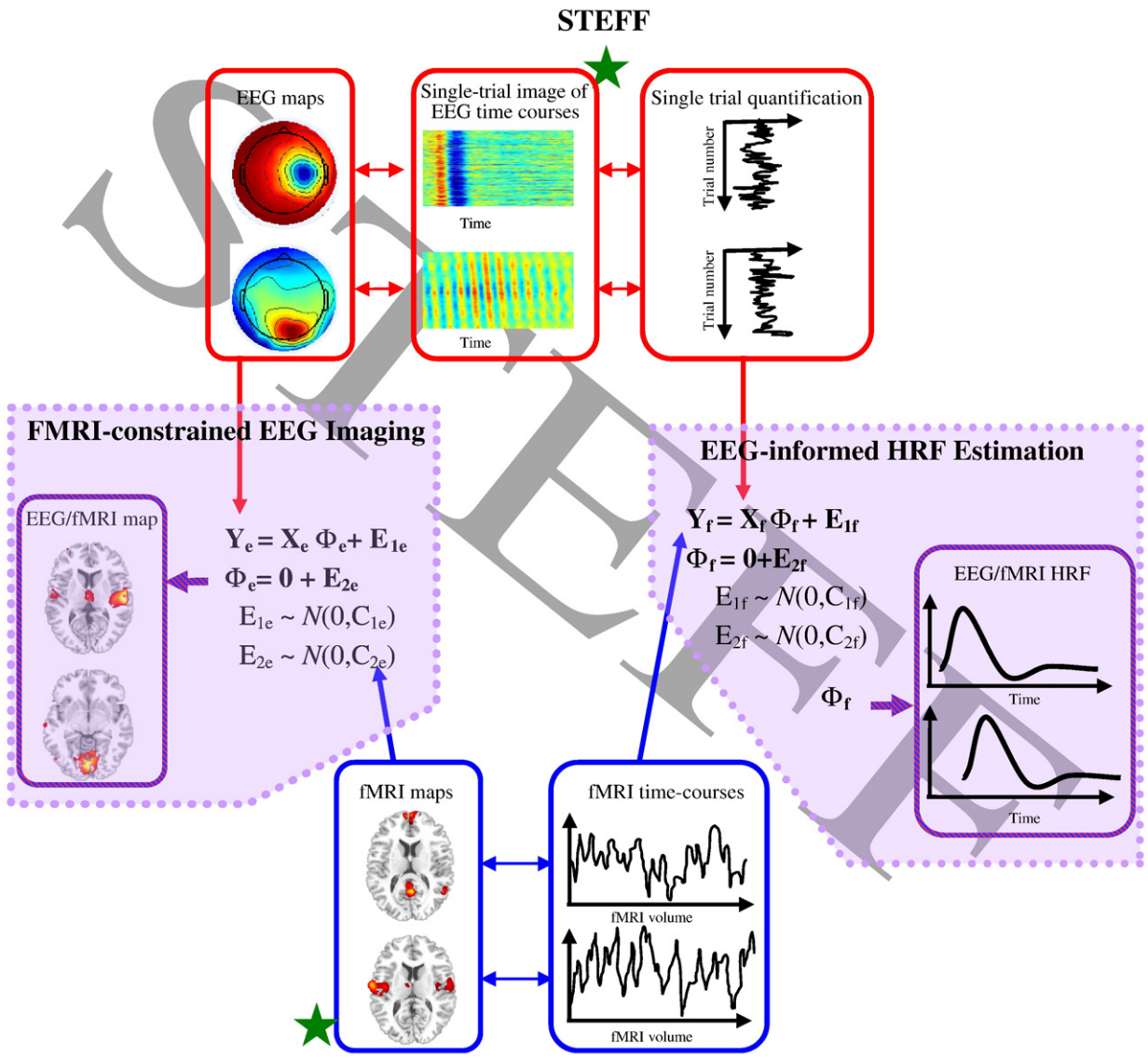

Fig. 2. STEFF employs fMRI constraints and EEG predictions in parallel for information integration in the unmixed space. FMRI sIC patterns (the bottom left panel) are employed as covariance priors (constraints) for EEG source distribution to find the voxel-wise description of the electrophysiological responses (left dashed area) of the topography of an EEG tIC (top left panel). The trial-by-trial dynamics ('single trial quantification' in the top right panel) extracted from EEG tIC time-courses (top center panel) are utilized to form the design matrix of the fMRI time-course (bottom right panel) of each fMRI sIC to estimate (predict) the hemodynamic response function (right dashed area), and then to reconstruct its neural fluctuation. ★: independent component.

the local coherence in source space and introduces the covariance component V_i^f as,

$$V_i^{\mathrm{f}} = \frac{1}{n_i}\sum_{j\in W(i)} q_j q_j^T, \tag{4}$$

where $W(i)$ is a set of activated nodes for ith sIC, n_i is the cardinality of $W(i)$, and q_j is the jth column of the Green function matrix G.

For the remaining source space outside the subspace generated by fMRI sIC, multiple sparse priors (Friston et al., 2008) are employed:

$$V_i^e = q_j q_j^T, \tag{5}$$

where q_j is evenly sampled from the remaining subspace. In light of its location, this approach can denote right hemisphere components as q_j^{right}, and left ones as q_j^{left}. Furthermore, homologues are added to form a bilateral component, $q_j^{\mathrm{both}} = q_j^{\mathrm{right}} + q_j^{\mathrm{left}}$, which models correlated sources in the two hemispheres.

In summary, the spatial priors for STEFF consist of two parts: fMRI sIC and multiple sparse priors (Friston et al., 2008). The effective number of fMRI sICs is automatically selected using an EB model optimization procedure (described in Section 2.4). After the optimization convergence, the conditional source estimate $\hat{\Phi}_e$ is the Maximum a Posteriori (MAP) estimate, or equivalently, the weighted minimum norm, the Tikhonov solution, and is given by:

$$\hat{\Phi}_e = \alpha C_{2e} X_e^T \left(\alpha X_e C_{2e} X_e^T + I_n\right)^{-1} Y_e. \tag{6}$$

The obtained hyperparameter γ_i encodes the link between $W(i)$ (the ith fMRI sIC) and Y_e (the topography of an EEG tIC).

EEG-informed HRF estimation (right dashed area in Fig. 2)

Many features of EEG data can be used as measures for each trial. A simple approach uses peak-to-peak amplitude differences of the tIC temporal course (Debener et al., 2005). A more sophisticated approach may employ machine learning to identify task-discriminating information (Goldman et al., 2009; Lei et al., 2009b). We propose a convenient approach for obtaining trial-to-trial EEG amplitude variances. Using singular value decomposition on the single trial

image of each EEG tIC ($N_t \times t_e$, number of trials times number of time points for a single trial; the top center panel in Fig. 2), the left singular vector, corresponding to the largest singular value, is defined as the single trial quantification (top right panel in Fig. 2).

We employ EB (or robust Bayesian GLM, cf. Marrelec and Benali, 2001) for the time-course of an fMRI sIC, Y_f, again for estimation of the hemodynamic response

$$\begin{array}{ll} Y_f = X_f\Phi_f + E_{1f} & E_{1f} \tilde{} N(0, C_{1f}) \\ \Phi_f = 0 + E_{2f} & E_{2f} \tilde{} N(0, C_{2f}), \end{array} \quad (7)$$

where $Y_f \in R^{n\times 1}$ is one time-course of the p fMRI sICs with n volumes (or time points), and $\Phi_f \in R^{d\times 1}$ is the unknown HRF for each time-course ($d = lm$, l: order of the convolution model; m: number of stimulus functions). The covariance of E_{1f} is $C_{1f} = \alpha^{-1} I_n$ and E_{2f} is C_{2f} as described below. $X_f \in R^{n\times d}$ is the design matrix, consisting of the lagged stimulus function matrix X_s. Given that $[x_1, x_2, \ldots, x_n]^T$, the ηth column of X_s, is an event time-course, then X_f is

$$X_f = \begin{bmatrix} \cdots & x_1 & 0 & 0 & 0 & \cdots \\ \cdots & x_2 & x_1 & 0 & 0 & \cdots \\ \cdots & \vdots & \vdots & \ddots & 0 & \cdots \\ \cdots & x_l & x_{l-1} & \cdots & x_1 & \cdots \\ \cdots & \vdots & \vdots & \vdots & \vdots & \cdots \\ \cdots & x_n & x_{n-1} & \cdots & x_{n-l+1} & \cdots \end{bmatrix}, \quad (8)$$

i.e., the $(\eta-1)l + 1$th to the ηlth columns of X_f contain the lagged ηth column of X_s. X_s consists of two kinds of stimulus functions (Eichele et al., 2008a):

$$X_s = \left[X_s^f X_s^e\right]. \quad (9)$$

The first stimulus function X_s^f encodes invariant evoked responses to target stimuli; the additional functions X_s^e encodes the 'single trial quantification' of the EEG tIC, where the single trial quantifications are first de-correlated using Schmidt-Gram orthogonalization from the nonspecific hemodynamic response to stimulus onsets, ensuring the specificity of inferences from the electrophysiological predictors.

The Φ_f in eq. (7) is assumed to fulfill a 'sparse restriction' that the number of stimulus vectors (i.e., columns in X_s) involved in Y_f generation should be as few as possible. This is realized by associating a hyperparameter γ_i ($i = 1, 2, \ldots, m$) with each HRF in Φ_f:

$$C_{2f} = \sum_{i=1}^{m} \gamma_i V_i, \quad (10)$$

where $V_i = \mathrm{diag}([\mathbf{0},\ldots,\mathbf{0}, Q^{-1}, \mathbf{0},\ldots,\mathbf{0}])$ is a $d \times d$ diagonal matrix whose diagonal elements are the inverse of the square matrix Q ($l \times l$ matrix defined in eq. (11)) for its ith element and $\mathbf{0}$ ($l \times l$ matrix of zeros) for others. In this way the relevance of each stimulus function can be determined separately via the optimization of the hyperparameter γ_i, and the irrelevant links between EEG tICs and the fMRI time-course will be effectively switched off. Q is the $l \times l$ concentration matrix of the Gaussian prior, chosen as the discrete second order differentiation matrix (Marrelec and Benali, 2001):

$$Q = \begin{bmatrix} 5 & -4 & 1 & 0 & & \cdots & & & 0 \\ -4 & 6 & -4 & 1 & 0 & & & & \\ 1 & -4 & 6 & -4 & 1 & 0 & & & \\ 0 & 1 & -4 & 6 & -4 & 1 & 0 & & \vdots \\ & \ddots & \ddots & \ddots & \ddots & \ddots & \ddots & \ddots & \\ \vdots & & 0 & 1 & -4 & 6 & -4 & 1 & 0 \\ & & & 0 & 1 & -4 & 6 & -4 & 1 \\ & & & & 0 & 1 & -4 & 6 & -4 \\ 0 & & \cdots & & & 0 & 1 & -4 & 5 \end{bmatrix}. \quad (11)$$

Q is a smooth constraint introduced to temporally regularize the problem. As stated by Marrelec et al. (2001), this approach has the advantage of not introducing bias into the estimation, since the constraints imposed are clearly derived from physiological requirements. Here, 'smooth' constraints for HRF and 'sparse' constraints between different stimulus functions are simultaneously imposed upon STEFF.

Omitting the second equation for the HRF constraint, the EB model in eq. (7) would be identical to the GLM (Friston et al., 1995) with a deconvolution method. This model has recently been applied to estimating the shape of the alpha band response function (de Munck et al., 2007).

Variational Bayesian inference

The 'fMRI-constrained EEG imaging' in eq. (1) and 'EEG-informed HRF estimation' in eq. (7) both adopt the same EB model. Hence both problems are solved using the same variational Bayesian inference. To ensure γ_i is non-negative, a hyperprior to the hyperparameters is introduced using a log-transform $\gamma_i = \exp(\phi_i)$ and a Gaussian hyperprior on $\phi = [\phi_1, \phi_2, \ldots, \phi_k]^T$ as $p(\phi) = N(\tau, \Gamma)$ (Friston et al., 2006). The generative model is then given by $Q = \{X, V\}$, and maximizing the model-evidence, $p(Y|Q)$, is equivalent to maximizing

$$\ln p(Y|Q) = \ln \int p(Y, \Phi|Q) d\Phi \approx F, \quad (12)$$

where F is the variational "free-energy" and is equal to

$$\begin{aligned} F = & -\frac{1}{2}\alpha(Y - X\Phi)^T(Y - X\Phi) - \frac{1}{2}\Phi^T C_2^{-1}\Phi - \frac{n}{2}\ln\alpha - \frac{n}{2}\ln|C_2^{-1}| \\ & + \frac{n}{2}\ln|\alpha X^T X + C_2^{-1}| - \frac{1}{2}(\phi - \tau)^T\Gamma^{-1}(\phi - \tau) - \frac{1}{2}\ln|\Gamma^{-1}| \\ & + \frac{1}{2}\ln|\Sigma^{-1}| + const, \end{aligned} \quad (13)$$

where *const* denotes a constant, Σ is the conditional covariance of the hyperparameters (see Friston et al., 2006, for details). F can be maximized using a standard variational scheme such as Expectation Maximization (EM) to furnish a tightly bound approximation to the log-evidence (Friston et al., 2008; Wipf and Nagarajan, 2009; Lei et al., 2009b), which also yields sparse matching of the 'common substrate' of neuronal activity.

Simulation

Our simulation involved the creation of sources, whose activity across the observation time window were reflected in the trial-by-

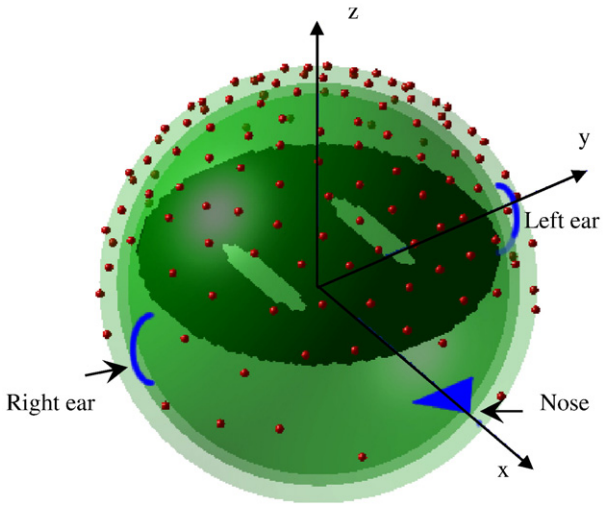

Fig. 3. Head model: 2452 voxels within a concentric three-sphere head model with 128 electrodes on the upper surface. The two holes in source slice are 'white matter.'

Table 1
Parameters in simulation.

EEG	fMRI
Sampling frequency: 100 Hz	Sampling frequency: 0.5 Hz (TR = 2 s)
Number of time samples: $t_e = 41$	Number of time samples: $t_f = 240$
Number of sensors: $n = 128$	Size of simulated HRF: $l = 17$
Gain matrix G: 3 spheres head model with analytic solution Sphere radii: [0.87 0.89 1]	HRF function: Gamma function with different onset time
Noise E_{1e}: Gaussian IID	Noise E_{1f}: Gaussian IID
Signal-to-noise ratio: $SNR_{EEG} = 1$	Signal-to-noise ratio: $SNR_{fMRI} = 0.1$

Number of trials: $N_t = 60$.
Number of dipoles/voxels: $n = 2452$.
Number of common sources: 4.
Number of modality specific source: 1.
Number of dipoles per source (S1–S6): [48 100 90 64 32 30].

trial modulation of two-dimensional fMRI spatial maps of 70×70 voxels with a field of view (FOV) of 200×200 mm^2 and a Z-axis of 18 mm. The repeat time (TR) of fMRI was 2 s. The size l of the simulated HRF was set to 17, corresponding to a 32 s (16×2 s) time window. Simultaneously, the EEG forward model was based on a concentric three-sphere head model with 128 electrodes placed on the upper hemisphere according to a pseudo 10–20 electrode setup (Fig. 3). The orientations of the EEG sources were fixed, and the lead-fields (X_e) for all sources were calculated analytically (Yao et al., 2004). The two 'white matter' holes were assumed to be blind for both EEG and fMRI. The event-related potentials (ERPs) consisted of 41 time points. The temporal sampling rate in an MR scanner is typically around 1 kHz, so that the current simulation corresponded to a 400 ms epoch after being down-sampled to 100 Hz. Other parameters are listed in Table 1.

In Fig. 4, the fifth row shows the assumed six analogously neurophysiological sources. From left to right: 'vision area' S1, 'default mode networks' S2, 'auditory cortex' S3, 'sensory networks' S4, 'left cognition area' S5 and 'right cognition area' S6. These areas were different in trial amplitudes across 60 trials (4th row). Trial amplitudes are functions with fast and slow dynamics induced by a stimulation paradigm: S1 is an increasing amplitude; S2 is a product of two sine waves with f1 = 1/120 Hz and f2 = 1/24 Hz; S3 shows a

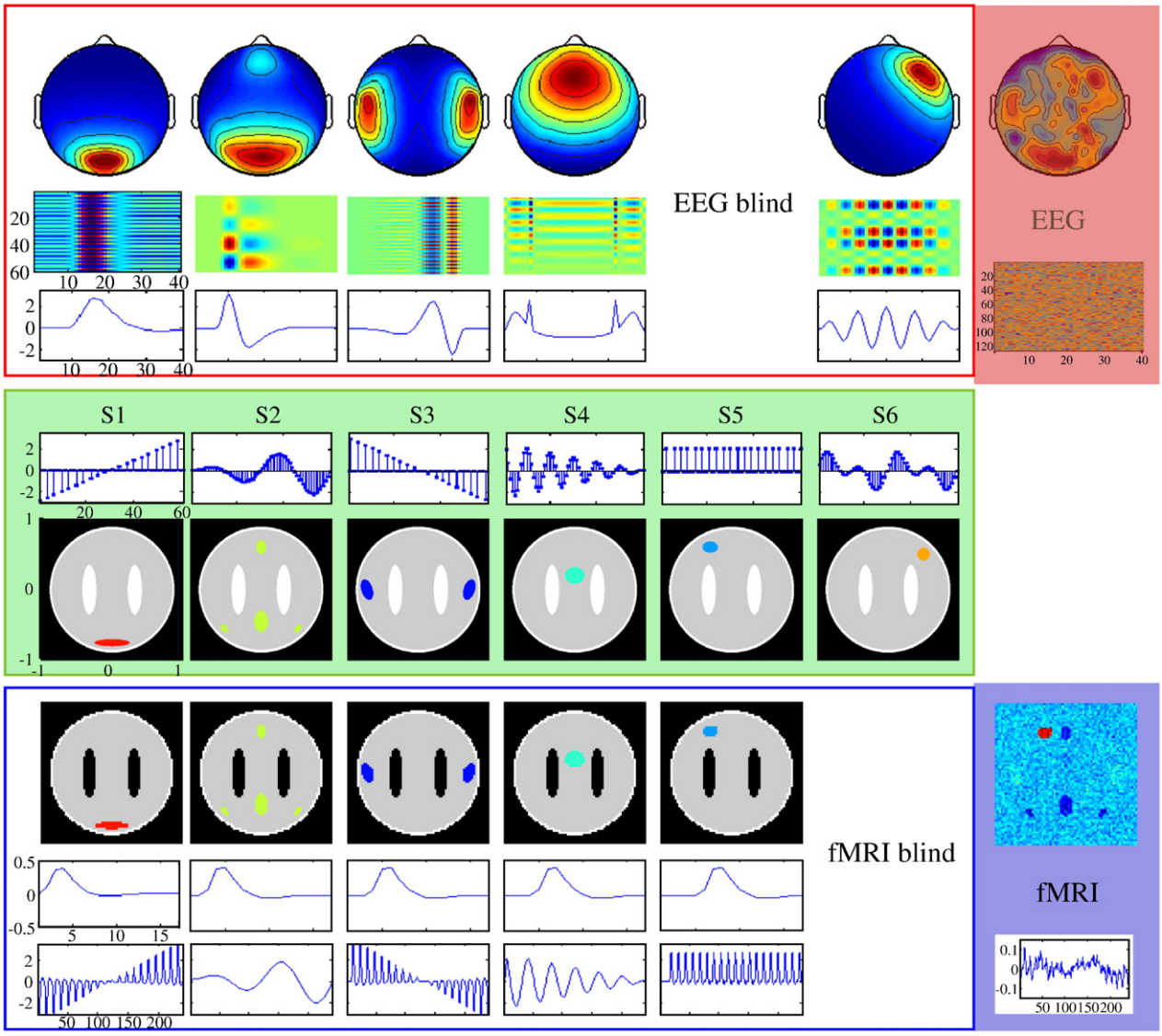

Fig. 4. Simulated sources of neuronal activity in simultaneous EEG/fMRI recordings. Columns from left to right are the sources 1–6 and their linear mixture (7th column). In total, eight key features are illustrated: for EEG, the features include scalp potential distribution (1st row), single trial images (2nd row) and ERP transient responses (3rd row). For neural activity, the features are single trial amplitude (4th row) and spatial distribution maps (5th row). For fMRI, the features are the spatial distribution (6th row), region-specific HRFs (7th row) and BOLD signals (8th row). Axes are the same for all columns and are shown on the leftmost plots. The rightmost panels are the simulated combined EEG/fMRI recordings.

decreasing amplitude; S4 is the product of two sine waves with f1 = 1/40 Hz and f2 = 1/480 Hz; S5 exhibits a fixed amplitude and S6 is the product of two sine waves with f1 = 1/60 Hz and f2 = 1/120 Hz.

These assumed active neural sources (green dashed areas in Fig. 4) yield scalp distributions and time-courses of EEG (red-bordered areas in Fig. 4), and time-courses of fMRI (blue-bordered areas in Fig. 4). S1–S4 are common sources for EEG and fMRI, and S5 and S6 are blind to EEG and fMRI, respectively. In total, eight key features are measured: for EEG, these include scalp potential distribution (1st row), single trial images (2nd row) and ERP transient responses (3rd row); for neural activity, the features included the single trial amplitude (4th row) and distribution maps (5th row); for fMRI, the features included the spatial distribution (6th row), region-specific HRFs (7th row) and BOLD signals (8th row). For EEG, single trial images (2nd row) were generated by multiplying each ERP transient response (3rd row) with the trial amplitude (4th row). Scalp potential distribution maps (1st row) were generated by computing the forward problem of each source pattern illustrated in the fifth row. For fMRI, BOLD signals were computed from the convolutions between trial amplitudes (4th row) and region-specific HRFs (7th row). The rightmost panels are examples for simulated data, which are entries for the analysis described below.

To demonstrate the feasibility of group ICA for various cases, only four of the five potential sources for each modality were randomly selected for each subject data set. Different Gaussian noise with independent and identical distributions (IID) was added to each data set. Here, we assumed a conservative signal-to-noise ratio (SNR) of 0.1 for fMRI and 1.0 for EEG. Such SNRs are consistent with typical experimental data. The rightmost panels in Fig. 4 represent the noisy data. Sixteen subject data-sets were simulated, corresponding to a medium-sized group study.

In the analysis stage, datasets were first pre-whitened and reduced using PCA. The dimensionality of the data (number of components) was estimated using the minimum description length criteria tool incorporated in the GIFT package, which attempts to minimize mutual information between components (for details see Li et al., 2007). For our implementation, the estimated number of components was five, and ICA was performed using projection pursuit as implemented in FastICA (Hyvarinen and Oja, 1997). Fig. 5 illustrates the result of group ICA for each modality. Group averaged components were used as input for the following STEFF analysis.

Table 2
EMD of source location and CC of HRF estimation for the five sources: S1, S2, S3, S4 and S5 (and average over all sources).

Method	Source 1	Source 2	Source 3	Source 4	Source 5	Average
EMD between estimated and true source location (mm)						
MNE	0.1892	0.1628	0.1219	0.2164	1.0767	0.3534
LORETA	0.3931	0.1342	0.1395	0.2041	0.8575	0.3457
MSP	0.1591	0.2172	0.1601	0.1884	0.7471	0.2944
fMRI-weighted MNE	0.1397	0.0764	0.0266	0.0481	1.4127	0.3407
STEFF	0.2315	0.0398	0.0393	0.0250	0.3709	0.1413
CCs between estimated HRF and true HRF (%)						
ML	46.09	0.07	86.85	1.48	70.42	40.98
STEFF	99.17	97.6	99.83	92.85	94	96.69

We compared STEFF to some other approaches in the estimations of Φ_e and Φ_f. For comparing source imaging between different approaches, we used minimum norm estimator (MNE) (Tikhonov and Arsenin, 1977), LORETA (Pascual-Marqui et al., 1994), MSP (Friston et al., 2008) and fMRI-weighted MNE (Liu et al., 1998).

For HRF estimation, the result of the STEFF analysis was compared with the simple maximum likelihood approach (ML; Friston et al., 1995; de Munck et al., 2007; Eichele et al., 2008b).

Spatial and temporal reconstruction results are detailed in Table 2. Here, the Earth Mover's Distance (EMD; Rubner et al., 2000) was used as the metric for image retrieval to evaluate the accuracy of the source localization method. CC was utilized to evaluate the accuracy of HRF estimation.

Fig. 6 shows the source localization results of the MNE, LORETA, MSP, fMRI-weighted MNE and STEFF approaches. In terms of EMD, STEFF performed substantially better than any of the other four methods, with or without fMRI information. The results confirmed that LORETA (0.3457) performed better than MNE (0.3534), although this difference was marginal. In Fig. 6, the reconstructed profile of

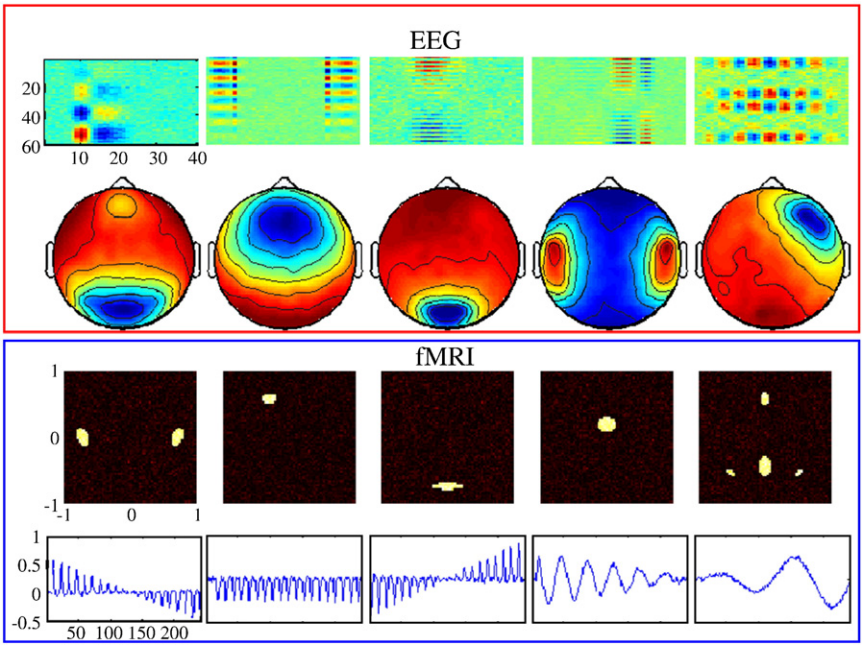

Fig. 5. The estimated independent components with four features for each source pattern: EEG single trial images (1st row), scalp potential distribution (2nd row), fMRI spatial distribution (3rd row) and the corresponding BOLD signals (4th row).

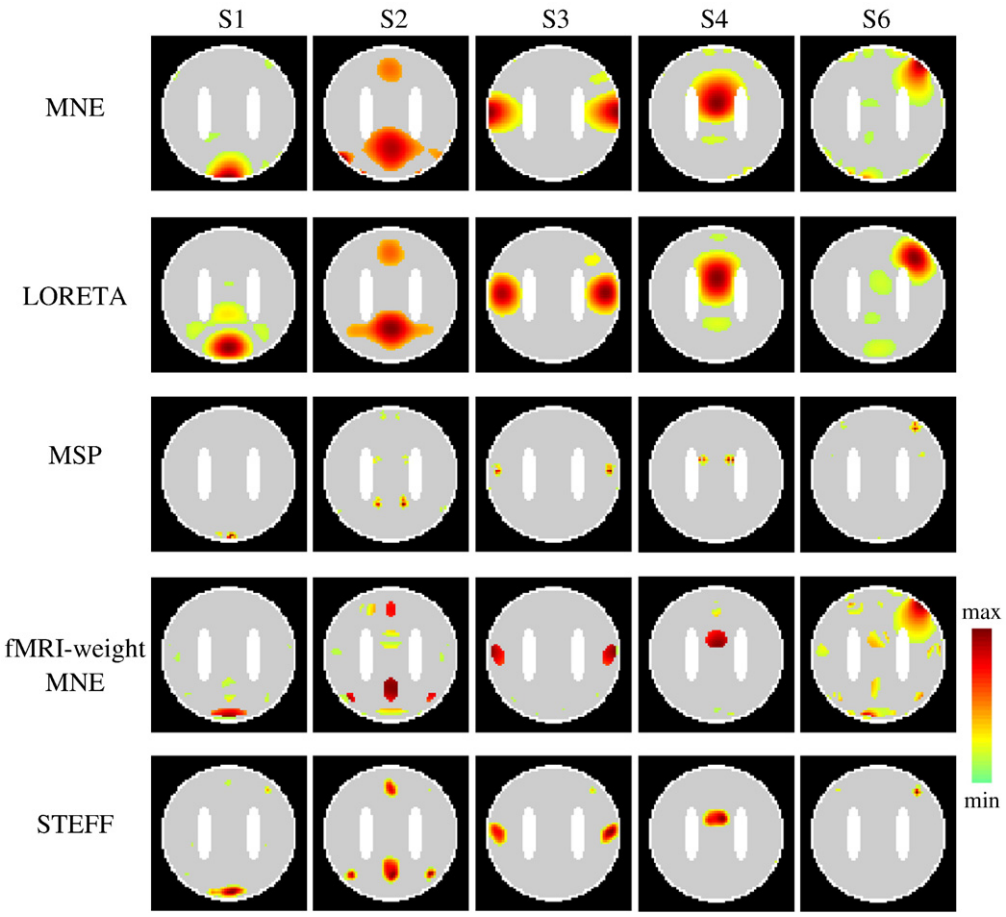

Fig. 6. Source localization results from left to right, corresponding to the assumed EEG sources S1–S4 and S6. From top to bottom: MNE, LORETA, MSP, fMRI-weighted MNE, and STEFF reconstructions. The maps are shown with threshold at the 1% quantile of the spatial distribution.

MNE was more superficial and spatially dispersed, particularly for sources S1 and S6. With 64 components per hemisphere ($3 \times 64 = 192$ components in total), MSP reconstructs all five sources with bilateral pairs of activity patterns. However, the support areas of this approach are very local and sparse. For fMRI-weighted MNE, the weights are 1 and 0.1 for visible and invisible fMRI source locations (Liu et al., 1998). The data are partly consistent with the true sources, but some irrelevant spatial patterns (for example, the S1 and S6 in Fig. 6) contaminated the results. The sources estimated by STEFF localized all the activated areas at their true positions. Specifically, the four activated areas in S2 were located at the correct positions only by STEFF.

As for the accuracy of the estimation of the HRF, STEFF reconstructed all the HRFs with an average CC of 96.69%, but for ML, this score was reduced to 40.98%. The hyperparameters of STEFF reflect the matching relationship between EEG and fMRI. Fig. 7 illustrates the spatial and temporal hyperparameters, where each column shows the relative contribution of each element in the left column to a component in the top row. The display of each column is normalized with its maximum. Importantly, it can be seen that the relative relation shown was accurate and sparse.

Discussion

In this work, we proposed a parallel approach to EEG/fMRI fusion, aiming to estimate both the common neural substrate of the responses measured by EEG and fMRI, and to identify modality-specific responses that were blind to one another. Below we discuss the technical details of STEFF, and outline potential future applications of our method.

Group ICA in STEFF

Group ICA is implemented in the current framework, and then group averaged components are employed for the concurrent EEG/fMRI fusion. A number of previous studies have reported that group ICA provides a straightforward and stringent solution for multi-subject component estimation (Calhoun et al., 2001; Schmithorst and Holland, 2004; Li et al., 2007). However, we must consider the potential risk that group ICA may miss a cognitive component of interest, producing misleading results.

Group ICA works well for sources that are spatially and temporally coherent across subjects and will readily detect such sources if they are present in approximately 10% of the sampled population (Schmithorst and Holland, 2004). Group tICA performed on EEG single trial time domain data is particularly suitable for detecting components that represent or contribute to event-related potentials visible in averaged data. Processes that are not time/phase-locked within and across subjects, such as background rhythms and induced activity are less appropriate. Correspondingly, for sICA on preprocessed fMRI data, regional BOLD responses that overlap across subjects can yield group-relevant components. Processes that occur in a spatially variable way over time in the recording of a single subject or that are principally spatially heterogeneous across subjects cannot be captured by this approach.

However, the choice of input data to group ICA is arbitrary, in that the original time or space domain data can be replaced with information such as power spectra or time-frequency data. This is particularly true when the fMRI correlates of EEG rhythms (Goldman et al., 2002) or event-related synchronization and desynchronization (Cheyne et al., 2008) are subject to study. Consequently, a useful

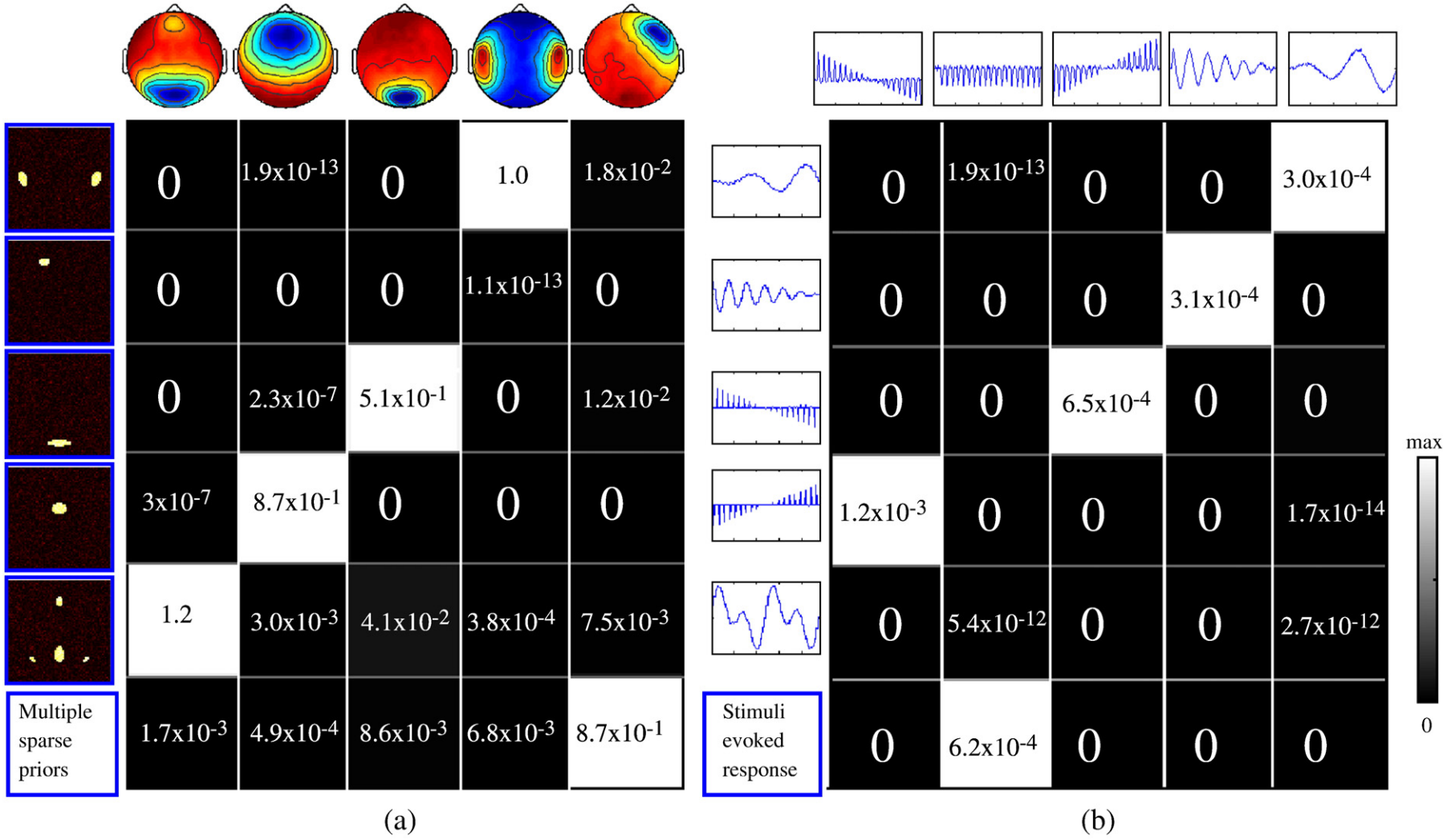

Fig. 7. The hyperparameters of STEFF reflect the matching relationships between EEG and fMRI. (a) The hyperparameters estimated in 'fMRI-constrained EEG Imaging' quantify the support from the EEG component (the top row) for each fMRI spatial pattern (the left column). (b) The hyperparameters estimated in "EEG-informed HRF Estimation" quantify the support from the fMRI component (the top row) for each EEG temporal pattern (the left column).

extension of the current framework would be the incorporation of multiple EEG and MRI features from single trial data (Calhoun et al., 2006) or to utilize other blind source separation methods (Langers, 2009). In any case, the STEFF framework appears to be useful for examining these features.

STEFF, data-driven and model-driven fusion

Generally, data-driven fusion approaches such as joint ICA are applied to data where specific hypotheses on spatial and temporal relationships are lacking, or are ill-specified, such as situations where traditional inference tests (Friston et al., 1995) are not justifiable or are too insensitive because of conservative significance thresholds. Simultaneous EEG/fMRI data adds additional problems to the analysis because of the involvement of two multivariate spaces and many necessary specifications. For example, there is an excessive degree of complexity in determining which channels would be sensitive to event-related function, which locations and latencies should be used to derive the event-related dynamics, which regions in fMRI activation would be expected, and which features should be utilized as fMRI predictors. In joint ICA, associations between the EEG/ERP and fMRI data are established during the decomposition process in a fused space, which inherently develops the relationships to each other in a more comprehensive fashion (Moosmann et al., 2008). In STEFF, since the blind unmixing of tICA for EEG, and sICA for fMRI data are complementary, all available EEG and fMRI data are used in the estimations. Subsequently, back-reconstruction semi-automatically produces maximally condensed components (the group averaged temporal and spatial components of EEG and fMRI, as shown in Fig. 2), and the EB model realizes flexible matching among the components.

Model-driven fusion is based on the formulation of an explicit biophysical model that illustrates post-synaptic potentials to EEG on one hand and BOLD signals on the other hand (Valdes-Sosa et al., 2009). Recent advances in physiological investigations approaches allow neuroscientists to develop sophisticated biophysical models for EEG/fMRI fusion. Bioelectric and metabolic activity has been modeled in neural populations based on dynamic causal models (Friston et al., 2003; Kiebel et al., 2006). Inversion of these integrative dynamic causal models might provide us with important insights into the nature and structure of cerebral activity and promote our understanding of neural mechanisms underlying perception and cognition. In STEFF, similar but less complicated models are involved: the EEG forward model and the BOLD convolution model. However, the model parameters are estimated using condensed components rather than channel-wise or voxel-wise EEG/fMRI data. Moreover, the results of STEFF may provide empirical constraints for hierarchical relationships among different levels of cortices (Garrido et al., 2007). In addition, STEFF provides a framework in which predictions from larger-scale computational models of electrophysiological and hemodynamic phenomena can be tested. For example, the approach may be used to locate the components that jointly reflect high-frequency EEG and low-frequency fMRI signals respectively (Deco et al., 2009).

STEFF is a hybrid approach, in which group ICA is used for generating data-driven hypotheses and spatial and temporal priors, which are then introduced to a model-driven approach (forward head model and neurovascular coupling) based on the hypotheses. The trial-to-trial modulations of EEG tICs are applied together to each fMRI time-course of the sICs to estimate the HRF function. Correspondingly, fMRI sICs are applied together to each EEG scalp topography of each tIC, to reconstruct the EEG source pattern. Traditionally, approaches for identifying shared neuronal sources that jointly express scalp electrophysiological and hemodynamic features or identifying IC-matching across modalities, were implemented with 'EEG-informed fMRI' and 'fMRI-constrained EEG'. Our proposed approach instead estimates hyperparameters among various components of EEG and fMRI within the parallel framework of STEFF.

Sparse mapping in different modalities

There are a variety of ways in which one can conceive the coupling between electrophysiology and hemodynamic signals. Linear regression between fMRI and EEG is typically used in combination with ICA to investigate links between modalities (e.g., Debener et al., 2005). In searching for such one-to-one mappings it is assumed that a particular EEG feature is related to a particular fMRI activity pattern. This conception involves an oversimplification, neglecting that in principle several fMRI patterns can affect several EEG signals.

In STEFF, we employ an EB model to link electrophysiology and hemodynamic signals. In the spatial domain, multiple fMRI-sIC patterns are input as priors for analyzing EEG topography. In the temporal domain, multiple EEG-tIC trial amplitudes are input as predictors for the fMRI time-course. This strategy enables sparse many-to-many mappings of the common neuronal substrate and temporal dynamic processes, which is more physiologically plausible than previous methods (Baudena et al., 1995; Halgren et al., 1995; Ritter and Villringer, 2006; Eichele et al., 2009).

Virtues of STEFF and its application

Currently accepted model-driven symmetrical fusion approaches require highly detailed large-scale computational modeling and explicit definitions of the common neuronal substrates generating both EEG and fMRI responses (Daunizeau et al., 2007; Deco et al., 2008; Valdes-Sosa et al., 2009). In consideration of this complexity, many researchers have employed meta-analysis using highly distilled data to examine convergent evidences. These analyses simply exhibit the results achieved by EEG source imaging and EEG-informed fMRI analysis (Esposito et al., 2005; Groening et al., 2009; Vulliemoz et al., 2009). In contrast to the two approaches discussed above, in STEFF we employ constraint and prediction simultaneously in a reciprocal way (Fig. 2). This method enjoys many advantages (illustrated in Fig. 8), discussed below.

- For source imaging, we take fMRI sICs as priors (the bottom area of column III in Fig. 8). This approach differs from other fMRI-constrained EEG imaging method (Liu et al., 1998; Dale et al., 2000; Liu et al., 2009) where fMRI activation is adopted equivalently. In

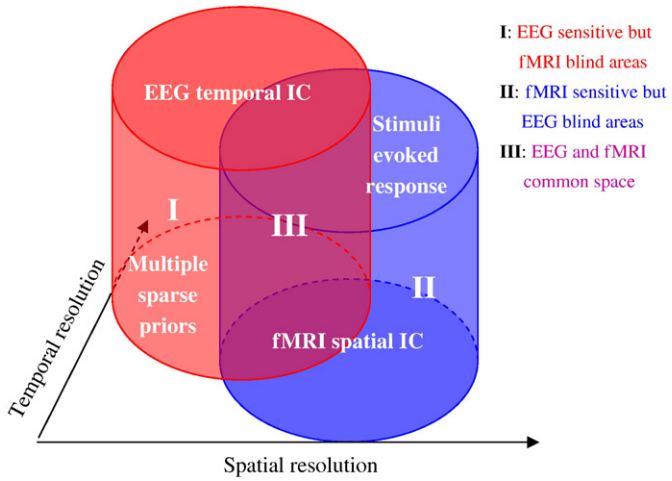

Fig. 8. The virtues of STEFF. With ICA, the "neuronal activity" is decomposed into two non-orthogonal sub-spaces: the red and blue columns contribute to the independent component of EEG and fMRI, respectively. The intersection column III of the red and blue columns defines the "common substrate" of neuronal activity. Conversely, the column I (respectively II) denotes the subspace of neuronal activity detected by EEG (or fMRI) that does not contribute to fMRI (or EEG) measurements. STEFF not only enables flexible matching in the column III but also reconstructs neuronal activity in I and II.

STEFF, the different spatial patterns (sICs) are given different weights by EB, thus the constraints are more flexible and realistic.
- For HRF estimation (the top area of column III in Fig. 8), apart from estimating HRF through the maximum likelihood approach (de Munck et al., 2007; Eichele et al., 2008b), the distinct advantage of STEFF is that the estimation is region-specific, and the estimated HRF is physiologically smoothed because of the adoption of a smoothness constraint.
- In examining the link between EEG and fMRI (shown in column III of Fig. 8), 'fMRI-constrained EEG imaging' enables multiple fMRI-sIC maps to match an EEG topography, and 'EEG-informed HRF estimation' enables multiple EEG-tIC trial amplitudes to match an fMRI time-course. As a result, more robust and flexible mappings are reconstructed as the common substrate of neuronal activity. Noticeably, the mappings are sparse, and flexible in facing mismatching situations of the spatial and temporal information. Moreover, the approach produces results that cover both temporal and spatial aspects of neuronal activity.
- Finally, subspaces (illustrated in columns I and II in Fig. 8) that are visible for only one modality can be examined using the STEFF approach. These areas are often omitted by other EEG/fMRI fusion studies, because typically only convergent evidence is considered of interest. However, these areas would be equally important for understanding various cognitive processes.

Because of the advantages shown above, STEFF is likely to provide important information furthering our understanding of various cognitive processes. STEFF shows particular promise for disentangling and visualizing the neural networks involved in processes where spatially and temporally widespread neuronal networks are activated (such as target detection in the auditory oddball task; Baudena et al., 1995; Halgren et al., 1995; Calhoun et al., 2006; Tian and Yao, 2008). Importantly, the definitions of events in STEFF can be very flexible, allowing the study of such diverse phenomena as cardiac triggering or interictal epileptic discharges (Marques et al., 2009). Thus, STEFF is a potential tool in clinical settings. As a parallel framework, STEFF also can be applied to resting-state data (Damoiseaux et al., 2006), where spontaneous specific frequency band power may be adopted as a regressor (single trial quantification in Fig. 2). In addition, based on the simultaneous spatial and temporal reconstruction of neuronal processes, this approach allows us to examine causal relations within active networks.

In conclusion, as a parallel framework for simultaneous EEG/fMRI recordings, STEFF not only provides a flexible tool for imaging the sources from EEG using information from fMRI data and to reconstruct the fMRI HRF using a design matrix from EEG data, but enables access to single modality-specific features of data. This approach can be applied to reveal common substrates between the two imaging modalities with convergent evidence, and to extend these insights to the blind areas of each modality. STEFF provides a mechanism for amending the problems of ignorance in ICA, the poor temporal resolution of fMRI and the poor spatial resolution of EEG. Techniques that are insufficient on their own can thus be used together efficiently to reveal a more complete dynamic picture of the complex brain-state fluctuations underlying cognitive and perceptual processes.

Acknowledgments

This project was funded by grants from the National Nature Science Foundation of China (30525030, 60736029, 30870655, 60701015) and the 863 project 2009AA02Z301.

References

Baillet, S., Mosher, J.C., Leahy, R.M., 2001. Electromagnetic brain mapping. IEEE Signal Process. Mag. 18, 14–30.

Baudena, P., Halgren, E., Heit, G., Clarke, J.M., 1995. Intracerebral potentials to rare target and distractor auditory and visual stimuli: III. Frontal cortex. Electroencephalogr. Clin. Neurophysiol. 94, 251–264.

Beckmann, C.F., Smith, S.M., 2004. Probabilistic independent component analysis for functional magnetic resonance imaging. IEEE Trans. Med. Imaging 23 (2), 137–152.

Calhoun, V.D., Adali, T., 2006. Unmixing fMRI with independent component analysis. IEEE Eng. Med. Biol. Mag. 25 (2), 79–90.

Calhoun, V.D., Adali, T., Pearlson, G.D., Pekar, J.J., 2001. A method for making group inferences from functional MRI data using independent component analysis. Hum. Brain Mapp. 14 (3), 140–151.

Calhoun, V.D., Adali, T., Pearlson, G.D., Kiehl, K.A., 2006. Neuronal chronometry of target detection: fusion of hemodynamic and event-related potential data. NeuroImage 30 (2), 544–553.

Calhoun, V.D., Liu, J., Adali, T., 2009. A review of group ICA for fMRI data and ICA for joint inference of imaging, genetic, and ERP data. NeuroImage 45, 163–172.

Chen, H., Yao, D., 2004. Discussion on the choice of separated components in fMRI data analysis by spatial independent component analysis. Magn. Reson. Imaging 22, 827–833.

Cheyne, D., Bells, S., Ferrari, P., Gaetz, W., Bostan, A.C., 2008. Self-paced movements induce high-frequency gamma oscillations in primary motor cortex. NeuroImage 42 (1), 332–342.

Dale, A.M., Halgren, E., 2001. Spatiotemporal mapping of brain activity by integration of multiple imaging modalities. Curr. Opin. Neurobiol. 11 (2), 202–208.

Dale, A.M., Liu, A.K., Fishl, B.R., Buckner, R.L., Belliveau, J.W., Lewine, J.D., Halgren, E., 2000. Dynamic statistical parametric neurotechnique mapping: combining fMRI and MEG for highresolution imaging of cortical activity. Neuron 26, 55–67.

Damoiseaux, J.S., Rombouts, S.A., Barkhof, F., Scheltens, P., Stam, C.J., Smith, S.M., Beckmann, C.F., 2006. Consistent resting-state networks across healthy subjects. Proc. Natl. Acad. Sci. U. S. A. 103, 13848–13853.

Daunizeau, J., Grova, C., Marrelec, G., Mattout, J., Jbabdi, S., Pélégrini-Issac, M., Lina, J.M., Benali, H., 2007. Symmetrical event-related EEG/fMRI information fusion in a variational Bayesian framework. NeuroImage 36 (1), 69–87.

Debener, S., Ullsperger, M., Siegel, M., Fiehler, K., von Cramon, D.Y., Engel, A.K., 2005. Trialby-trial coupling of concurrent electroencephalogram and functional magnetic resonance imaging identifies the dynamics of performance monitoring. J. Neurosci. 25, 11730–11737.

Debener, S., Ullsperger, M., Siegel, M., Engel, A.K., 2006. Single-trial EEG–fMRI reveals the dynamics of cognitive function. Trends Cogn. Sci. 10 (12), 558–563.

Deco, G., Jirsa, V.K., Robinson, P.A., Breakspear, M., Friston, K., 2008. the dynamic brain: from spiking neurons to neural masses and cortical fields. PLoS Comput. Biol. 4 (8), e1000092. doi:10.1371/journal.pcbi.1000092.

Deco, G., Jirsa, V., McIntosh, A.R., Sporns, O., Kotter, R., 2009. Key role of coupling, delay, and noise in resting brain fluctuations. Proc. Natl. Acad. Sci. U. S. A. 106, 10302–10307.

de Munck, J.C., Goncalves, S.I., Huijboom, L., Kuijer, J.P., Pouwels, P.J., Heethaar, R.M., Lopes da Silva, F.H., 2007. The hemodynamic response of the alpha rhythm: an EEG/fMRI study. NeuroImage 35, 1142–1151.

Eichele, T., Specht, K., Moosmann, M., Jongsma, M.L., Quiroga, R.Q., Nordby, H., Hugdahl, K., 2005. Assessing the spatiotemporal evolution of neuronal activation with single-trial event-related potentials and functional MRI. Proc. Natl. Acad. Sci. U. S. A. 102, 17798–17803.

Eichele, T., Calhoun, V.D., Moosmann, M., Specht, K., Jongsma, M.L., Quiroga, R.Q., Nordby, H., Hugdahl, K., 2008a. Unmixing concurrent EEG-fMRI with parallel independent component analysis. Int. J. Psychophysiol. 67, 222–234.

Eichele, T., Debener, S., Calhoun, V.D., Specht, K., Engel, A.K., Hugdahl, K., von Cramon, D.Y., Ullsperger, M., 2008b. Prediction of human errors by maladaptive changes in event-related brain networks. Proc. Natl. Acad. Sci. U. S. A. 105, 6173–6178.

Eichele, T., Calhoun, V.D., Debener, S., 2009. Mining EEG-fMRI using independent component analysis. Int. J. Psychophysiol. 73 (1), 53–61.

Esposito, F., Scarabino, T., Hyvarinen, A., Himberg, J., Formisano, E., Comani, S., Tedeschi, G., Goebel, R., Seifritz, E., Di Salle, F., 2005. Independent component analysis of fMRI group studies by self-organizing clustering. NeuroImage 25, 193–205.

Friston, K.J., Holmes, A.P., Worsley, K.J., Poline, J.-P., Frith, C.D., Frackowiak, R.S., 1995. Statistical parametric maps in functional imaging: a general linear approach. Hum. Brain Mapp. 2, 189–210.

Friston, K.J., Harrison, L., Penny, W., 2003. Dynamic causal modelling. NeuroImage 19, 1273–1302.

Friston, K., Henson, R., Phillips, C., Mattout, J., 2006. Bayesian estimation of evoked and induced responses. Hum. Brain Mapp. 27, 722–735.

Friston, K.J., Harrison, L., Daunizeau, J., Kiebel, S.J., Phillips, C., Trujillo-Bareto, N., Henson, R.N., Flandin, G., Mattout, J., 2008. Multiple sparse priors for the M/EEG inverse problem. NeuroImage 39, 1104–1120.

Garrido, M.I., Kilner, J.M., Kiebel, S.J., Friston, K.J., 2007. Evoked brain responses are generated by feedback loops. Proc. Natl. Acad. Sci. U. S. A. 104, 20961–20966.

GIFT, 2008: Group ICA of fMRI Toolbox (GIFT). http://icatb.sourceforge.net/, Website, http://icatb.sourceforge.net/.

Goldman, R.I., Stern, J.M., Engel, J., Cohen, M.S., 2002. Simultaneous EEG and fMRI of the alpha rhythm. Neuroreport 13, 2487–2492.

Goldman, R.I., Cheng-Yu, W., Philiastides, M.G., Gerson, A.D., Friedman, D., Brown, T.R., Sajda, P., 2009. Single-trial discrimination for integrating simultaneous EEG and fMRI: Identifying cortical areas contributing to trial-to-trial variability in the auditory oddball task. NeuroImage 47 (1), 136–147.

Groening, K., Brodbeck, V., Moeller, F., Wolff, S., van Baalen, A., Michel, C.M., Jansen, O., Boor, R., Wiegand, G., Stephani, U., Siniatchkin, M., 2009. Combination of EEG-fMRI and EEG source analysis improves interpretation of spike-associated activation networks in paediatric pharmacoresistant focal epilepsies. NeuroImage 46 (3), 827–833.

Halgren, E., Baudena, P., Clarke, J.M., Heit, G., Liegeois, C., Chauvel, P., Musolino, A., 1995. Intracerebral potentials to rare target and distractor auditory and visual stimuli. I. Superior temporal plane and parietal lobe. Electroencephalogr. Clin. Neurophysiol. 94, 191–220.

Harrison, L.M., Penny, W., Ashburner, J., Trujillo-Barreto, N., Friston, K.J., 2007. Diffusion-based spatial priors for imaging. NeuroImage 38, 677–695.

Helmholtz, H.L.F., 1853. Ueber einige Gesetze der Vertheilung elektrischer Ströme in körperlichen Leitern mit Anwendung aud die thierisch-elektrischen Versuche. Ann. Phys. Chem. 9, 211–233.

Hyvarinen, A., Oja, E., 1997. A fast fixed-point algorithm for independent component analysis. Neural Comput. 9 (7), 1483–1492.

Ives, J.R., Warach, S., Schmitt, F., Edelman, R.R., Schomer, D.L., 1993. Monitoring the patient's EEG during echo planar MRI. Electroencephalogr. Clin. Neurophysiol. 87 (6), 417–420.

Kiebel, S.J., David, O., Friston, K.J., 2006. Dynamic causal modelling of evoked responses in EEG/MEG with lead field parameterization. NeuroImage 30 (4), 1273–1284.

Langers, D.R., 2009. Blind source separation of fMRI data by means of factor analytic transformations. NeuroImage 47 (1), 77–87.

Laufs, H., Daunizeau, J., Carmichael, D.W., Kleinschmidt, A., 2008. Recent advances in recording electrophysiological data simultaneously with magnetic resonance imaging. NeuroImage 40, 515–528.

Lei, X., Chen, A., Xu, P., Yao, D., 2009a. Gaussian source model based iterative algorithm for EEG source imaging. Comput. Biol. Med. 39, 978–988.

Lei, X., Yang, P., Yao, D., 2009b. An empirical Bayesian framework for brain computer interfaces. IEEE Trans. Neural Syst. Rehab. Eng. doi:10.1109/TNSRE.2009.2027704

Lei, X., Yao, D., 2009. EEG source localization based on multiple fMRI spatial patterns. The 2nd International Conference on Cognitive Neurodynamics. Hangzhou, China.

Li, Y., Adali, T., Calhoun, V.D., 2007. Estimating the number of independent components for fMRI data. Hum. Brain Mapp. 28 (11), 1251–1266.

Liu, A.K., Belliveau, J.W., Dale, A.M., 1998. Spatiotemporal imaging of human brain activity using functional MRI constrained magnetoencephalographic data: Monte Carlo simulations. Proc. Natl. Acad. Sci. U. S. A. 95, 8945–8950.

Liu, Z., Zhang, N., Chen, W., He, B., 2009. Mapping the bilateral visual integration by EEG and fMRI. NeuroImage 46, 989–997.

Logothetis, N.K., Pauls, J., Augath, M., Trinath, T., Oeltermann, A., 2001. Neurophysiological investigation of the basis of the fMRI signal. Nature 412 (6843), 150–157.

Makeig, S., Debener, S., Onton, J., Delorme, A., 2004. Mining event-related brain dynamics. Trends in Cognitive Science 8 (5), 204–210.

Marques, JP., Rebola, J., Figueiredo, P., Pinto, A., Sales, F., 2009. Castelo-Branco M. ICA decomposition of EEG signal for fMRI processing in epilepsy. Hum. Brain Mapp. Jan 26. [electronic publication ahead of print].

Marrelec, G., Benali, H., 2001. Non-parametric Bayesian deconvolution of fMRI hemodynamic response function using smoothing prior. NeuroImage 13 (6), S194.

Martinez-Montes, E., Valdes-Sosa, P.A., Miwakeichi, F., Goldman, R.I., Cohen, M.S., 2004. Concurrent EEG/fMRI analysis by multiway partial least squares. NeuroImage 22, 1023–1034.

McKeown, M.J., Makeig, S., Brown, G.G., Jung, T.P., Kindermann, S.S., Bell, A.J., Sejnowski, T.J., 1998. Analysis of fMRI data by blind separation into independent spatial components. Hum. Brain Mapp. 6, 160–188.

Moosmann, M., Eichele, T., Nordby, H., Hugdahl, K., Calhoun, V.D., 2008. Joint independent component analysis for simultaneous EEG-fMRI: principle and simulation. Int. J. Psychophysiol. 67, 212–221.

Nunez, P.L., 1995. Neocortical Dynamics and Human EEG Rhythms. Oxford Univ. Press, New York.

Pascual-Marqui, R.D., Michel, C.M., Lehmann, D., 1994. Low resolution electromagnetic tomography: a new method for localizing electrical activity in the brain. Int. J. Psychophysiol. 18, 49–65.

Phillips, C., Mattout, J., Rugg, M.D., Maquet, P., Friston, K.J., 2005. An empirical Bayesian solution to the source reconstruction problem in EEG. NeuroImage 24, 997–1011.

Ritter, P., Villringer, A., 2006. Simultaneous EEG-fMRI. Neurosci. Biobehav. Rev 30 (6), 823–838.

Rubner, Y., Tomasi, C., Guibas, L.J., 2000. The Earth Mover's Distance as a Metric for Image Retrieval. Int. J. Comput. Vis. 40 (2), 99–121.

Schmithorst, V.J., Holland, S.K., 2004. Comparison of three methods for generating group statistical inferences from independent component analysis of functional magnetic resonance imaging data. J. Magn. Reson. Imaging 19 (3), 365–368.

Tian, Y., Yao, D., 2008. A study on the neural mechanism of inhibition of return by the event-related potential in the Go/Nogo task. Biol. Psychol. 79 (2), 171–178.

Trujillo-Barreto, N., Martinez-Montes, E., Melie-Garcia, L., Valdes-Sosa, P., 2001. A symmetrical Bayesian model for fMRI and EEG/MEG neuroimage fusion. Int. J. Bioelectromagn. 3 (Available at http://www.ijbem.org/volume3/number1/toc.htm).

Valdes-Sosa, P.A., Sanchez-Bornot, J.M., Sotero, R.C., Iturria-Medina, Y., eman-Gomez, Y., Bosch-Bayard, J., Carbonell, F., Ozaki, T., 2009. Model driven EEG/fMRI fusion of brain oscillations. Hum. Brain Mapp. 30 (9), 2701–2721.

Vulliemoz, S., Thornton, R., Rodionov, R., Carmichael, D.W., Guye, M., Lhatoo, S., McEvoy, A.W., Spinelli, L., Michel, C.M., Duncan, J.S., Lemieux, L., 2009. The spatio-temporal mapping of epileptic networks: combination of EEG-fMRI and EEG source imaging. NeuroImage 46 (3), 834–843.

Warbrick, T., Mobascher, A., Brinkmeyer, J., Musso, F., Richter, N., Stoecker, T., Fink, G.R., Shah, N.J., Winterer, G., 2009. Single-trial P3 amplitude and latency informed event-related fMRI models yield different BOLD response patterns to a target detection task. NeuroImage. doi:10.1016/j.neuroimage.2009.05.082.

Wipf, D., Nagarajan, S., 2009. A unified Bayesian framework for MEG/EEG source imaging. NeuroImage 44, 947–966.

Yao, D., 2001. A method to standardize a reference of scalp EEG recordings to a point at infinity. Physiol. Meas. 22, 693–711.

Yao, D., Yin, Z., Tang, X., Arendt-Nielsen, L., Chen, A.C., 2004. High-resolution electroencephalogram (EEG) mapping: scalp charge layer. Phys. Med. Biol. 49 (22), 5073–5086.

Yao, D., Wang, L., Oostenveld, R., Nielsen, K., Arendt-Nielsen, L., Chen, A., 2005. A comparative study of different references for EEG spectral mapping the issue of neutral reference and the use of infinity reference. Physiol. Meas. 26, 173–184.